12th International Conference on CANDU Fuel
Holiday-Inn Waterfront Hotel
Kingston, Ontario, Canada, 2013 September 15-18

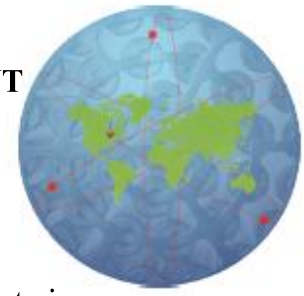

FEASIBILITY STUDY OF MODELING A CANDU FUEL ELEMENT USING A MULTIPHYSICS OBJECT-ORIENTED SIMULATION ENVIRONMENT

K. Gamble[1], A. Williams 2[2] and P.K. Chan[1]
[1]Royal Military College of Canada, Kingston, Ontario, Canada
Royal Miliatry College of Canada, PO Box 17000, Station Forces, Kingston, Ontario, Canada, Phone: 613-541-6000 x. 6667, Email: Kyle.Gamble@rmc.ca
[2]Atomic Energy of Canada Limited, Chalk River, Ontario, Canada

ABSTRACT

The first phase of the feasibility study of using a Multiphysics Object-Oriented Simulation Environment (MOOSE) for modeling a CANDU fuel element is presented. A two dimensional model of a fuel pellet and sheath was created to examine the contact algorithm within MOOSE. The results obtained show the expected behaviour of contact pressure and penetration in 2D. Preliminary results for a 3D model of a quarter fuel pellet and sheath are provided but at present contain anomalies currently being investigated. The next steps in the feasibility study are outlined.

1. Introduction

Predictive modeling capabilities provide valuable insight into nuclear fuel behaviour from the perspectives of the industry and regulators. Computational constraints arise when the geometrical size and physical complexity of the model increase. Multiple computational models have been generated that are detailed in either geometry or physics but not both simultaneously because of the difficulty and cost associated with large complex models using current commercial software. For example the finite element analysis package ANSYS requires a (High Performance Computer) HPC license to run on multiple cores. The cost of this license increases as the number of cores to be used increases.

A variety of researchers have developed finite element models for predicting the behavior of nuclear fuel of varying geometrical size and physical complexity using commercial software. Prudil et al. have created a physically complex model involving heat generation and transport, thermal expansion, elastic strain, densification, fission product swelling, contact, grain growth, fission gas release, gas and coolant pressure and sheath creep of a quarter cross-section of a fuel pellet and sheath in the radial and axial dimensions. The results obtained were in excellent agreement with experiment and Industry Standard Toolset ELESTRES [1]. Bell et al. examined the thermal deformation of an entire 37 CANDU fuel bundle. The fuel elements were modeled using beam elements, the bearing and spacer pads were ignored, and inter-element contact was not modeled. Average fuel temperatures were in reasonable agreement with ELESTRES and bundle deformation results were in excellent agreement with the BOW code and out of reactor experiments [2]. Williams et al. at Atomic Energy of Canada Limited (AECL) have developed a complex-three-dimensional model of a quarter of a fuel element using ANSYS. Results are in good agreement with experimental results however convergence issues are encountered when the sheath detaches from the pellets during cooling [3]. The final model of great interest to the industry is a full 37-element bundle model, with inter-element contact as well as the details of the pellets in each fuel

element, with computational fluid dynamics (CFD) used for fuel subchannel conditions. Although the models described above are useful and correct for their particular application, they cannot be extended to geometric large and physically complex models due to the numerical instabilities introduced, or computational resources required using the software employed. As the geometrical size of the model increases, the amount of physics can be included must decline. Therefore, a more computationally efficient and robust solution method is required.

Idaho National Laboratory (INL) has developed the MOOSE framework used for solving fully coupled differential equations built upon a Jacobian Free Newton-Krylov (JFNK) method. The MOOSE framework is inherently parallel allowing for large models to be run on multiple processors with no additional cost. To determine the capabilities of MOOSE, an analysis of the contact algorithm employed was completed. The dependence of the interpenetration of the pellet and sheath, and the interfacial pressure between the two bodies as a function of the penalty factor was determined for both cases in 2D and 3D. The penalty factor is the spring constant of the artificial spring that is introduced between the contacting surfaces, which relates the interpenetration distance to the contact force. Then using the nodal area of each individual node, the contact pressure at that location can be determined from the contact force. Temperature profiles were also produced. The preliminary results of this analysis are provided in this paper.

2. The Computational Framework

It is important to note that MOOSE is only a computational framework to solve complex physics problems and contains no physics of its own. The kernels, boundary conditions, and material properties are contained within other applications built upon the MOOSE framework. The developers of MOOSE insist that any application built upon the framework is also given an animal name. The Extended Library of Kernels (ELK) houses general physics that is applicable to a variety of research fields such as solid mechanics, Navier-Stokes, heat transfer and contact. Built on top of ELK is FOX which is a more specialized library containing general nuclear performance equations. It is upon FOX that the HORizontal nuclear fuel Simulation Environment (HORSE) developed within this work is being built. Additional MOOSE based applications are built upon ELK that examine problems in a variety of fields of science and engineering including but not limited to, reactive transport and microstructure evolution.

Current commercial software packages such as ANSYS and COMSOL use the Newton-Raphson method to solve the system of fully coupled nonlinear equations. The Newton-Raphson technique has fast convergence properties but requires the analytical computation of what is known as the Jacobian matrix, in which elements are analytical derivatives of every nonlinear equation with respect to every field variable in the system. To avoid the large computational requirements to perform analytical derivatives and to store the Jacobian, MOOSE uses what is known as a Jacobian-Free Newton Krylov (JFNK) technique for solving the system of equations. The details of the Jacobian-Free technique are given in the following subsections.

2.1 Newton's Method

Newton's method is a root finding method of solving nonlinear equations. For a nonlinear equation of a single variable Newton's method yields

$$x_{n+1} = x_n + \delta x_{n+1} \quad \textbf{(1)}$$

where x_n is the current value of the variable, x_{n+1} is the next iteration of the variable and

$$\delta x_{n+1} = -\frac{f(x_n)}{f'(x_n)} \quad \textbf{(2)}$$

For a single variable it is quite simple to solve this equation, computational constraints can become a factor when solving a system of nonlinear equations as one obtains

$$\mathbf{J}(\mathbf{u}_n)\delta\mathbf{u}_{n+1} = -\mathbf{R}(\mathbf{u}_n) \quad \textbf{(3)}$$

where **R** is the residual vector given by the weak form of each nonlinear equation and **J** is the Jacobian matrix with its elements given by

$$J_{ij} = \frac{\partial R_i(\mathbf{u}_n)}{\partial u_j} \quad \textbf{(4)}$$

It can be seen from equation (4) that the Jacobian matrix is a complex object to find. The elements of the Jacobian are given by taking the partial derivative of each nonlinear equation in the system with respect to each variable being solved for in the system. Derivative calculations can be difficult and error prone. Therefore, a method that eliminates the need to solve for the Jacobian explicitly is desired. Equation (3) is essentially a system of linear equations that need to be solved to obtain $\delta\mathbf{u}_{n+1}$ which is then used to solve the nonlinear system as given by equation (1) but in vector form. The system of linear equations is solved using a Krylov solver.

2.2 Krylov Method

MOOSE employs the Generalized Minimized Residual (GMRES) iterative Krylov solver. In this method the representation of the solution to the linear system of equations is given by

$$\delta\mathbf{u}_{n+1}^k = a_0\mathbf{r}_0 + a_1\mathbf{J}\mathbf{r}_0 + a_2\mathbf{J}^2\mathbf{r}_0 + \ \ldots + a_k\mathbf{J}^k\mathbf{r}_0 \quad \textbf{(5)}$$

where *k* is the Krylov iteration number. Using equation (5), the Krylov method is iterated until the right-hand side of equation (3) is within some specified tolerance of zero. By examining equation 5 it can be seen that for every Krylov iteration an additional term is added to the right hand side of the equation. Once that is achieved the nonlinear step is said to have converged. Equation 5 also illustrates that only the action of the Jacobian on a vector is required which can be approximated by a finite difference of the form [4]

$$\mathbf{J}\mathbf{v} \approx \frac{\mathbf{R}(\mathbf{u}+\varepsilon\mathbf{v}) - \mathbf{R}(\mathbf{u})}{\varepsilon} \quad \textbf{(6)}$$

where,

$$\varepsilon = \frac{1}{N\|\mathbf{v}\|_2}\sum_{i=1}^{N} bu_i \quad \textbf{(7)}$$

and b = 1.0 x 10^{-8}, N is the number of unknowns, and $\mathbf{v}$ is a Krylov vector (i.e. $\mathbf{v} \in (\mathbf{r}_0, \mathbf{J}\mathbf{r}_0, \mathbf{J}^2\mathbf{r}_0, \ldots)$). The advantage of using this approximation is that a large amount of computational time is saved as analytical derivatives are not required to compute **J** and no memory space is needed to store the potentially large **J** matrix. However, since the GMRES solver stores all of the previous Krylov vectors in memory, it is necessary to minimize the number of Krylov iterations to solve the linear system of equations [5].

2.3 Preconditioning

Minimization of the Krylov iterations is accomplished by using right preconditioning. For each Krylov iteration preconditioning is achieved by solving

$$\mathbf{J}(\mathbf{u}_n^k)\mathbf{P}^{-1}\mathbf{P}\delta\mathbf{u}_{n+1}^k = -\mathbf{R}(\mathbf{u}_n^k) \quad \textbf{(8)}$$

where $\mathbf{P}$ represents the preconditioning matrix and $\mathbf{P}^{-1}$ the inverse of the preconditioning matrix. Right preconditioning is achieved through a two-step process. The first step is to solve

$$\mathbf{J}(\mathbf{u}_n^k)\mathbf{P}^{-1}\mathbf{w} = -\mathbf{R}(\mathbf{u}_n^k) \quad \textbf{(9)}$$

for $\mathbf{w}$. Then solve

$$\delta\mathbf{u}_{n+1}^k = \mathbf{P}^{-1}\mathbf{w} \quad \textbf{(10)}$$

for $\delta\mathbf{u}_{n+1}^k$,which yields the right preconditioned form of equation 6 given by [4]

$$\mathbf{J}\mathbf{P}^{-1}\mathbf{v} \approx \frac{\mathbf{R}(\mathbf{u}+\varepsilon\mathbf{P}^{-1}\mathbf{v}) - \mathbf{R}(\mathbf{u})}{\varepsilon} \quad \textbf{(11)}$$

By choosing the correct preconditioner $\mathbf{P}^{-1}$ the number of Krylov iterations in the GMRES method can be minimized. The difficulty that arises is to choose the correct type of preconditioner for the nonlinear system under consideration. There are many options typically used such as Newton-Krylov-Schwarz, Multigrid and physics-based preconditioners [4]. A common physics based preconditioner is operator splitting. Operator splitting refers to the splitting of the solution process based on different types of physics [6] The types of preconditioning offered in MOOSE are included in the Portable, Extensible Toolkit for Scientific Computation (PETSc) library. The details of the different preconditioners can be found in the PETSc User Manual [7]. In the contact analysis completed in this work a Single Matrix Preconditioner (SMP) was used. The MOOSE developers advise new users to use the default block diagonal preconditioner until convergence issues are encountered [8]. The SMP was chosen for this work because convergence issues were

being encountered when using the default preconditioner. The choice of SMP over other available preconditioners was that it has been used in numerous example problems of the MOOSE based application BISON, which simulates the nuclear fuel performance of light water reactors fuel rods and other fuel types.

3. Assessment Methodology

The first step of the feasibility analysis was to examine the robustness and behaviour of the contact algorithm employed in MOOSE. To complete the analysis, both a two-dimensional and three-dimensional model were produced to determine if the contact algorithm behaved differently in the different dimensions. Both models contained constant material properties and heat generation to isolate the contact behaviour from other effects such as temperature dependent material properties, non-uniform heat generation. For the contact analysis, constant material properties were used. The next subsections provide in detail the geometry and mesh, material properties, and boundary conditions for both the two and three-dimesional cases.

4. Model Development

In thermomechanical modeling the variables of interest are temperatures and displacements. Temperature is determined using energy conversation through the heat conduction equation given by

$$\rho C_p \frac{\partial T}{\partial t} + \nabla \cdot \mathbf{q} - e_f \dot{F} = 0 \tag{12}$$

where

$$\mathbf{q} = -k \nabla T \tag{13}$$

and ρ is the density, C_p is the specific heat, and k is the thermal conductivity of the material. In the internal heat generation term e_f is the energy produced per fission within the fuel and $\dot{F}$ is a volumetric fission rate that is a function of space and time. Momentum conversation is determined at each time increment by Cauchy's equation which states

$$\nabla \cdot \boldsymbol{\sigma} + \rho \mathbf{g} = 0 \tag{14}$$

where $\boldsymbol{\sigma}$ is the Cauchy stress tensor given by

$$\begin{bmatrix} \sigma_{xx} & \sigma_{xy} & \sigma_{xz} \\ \sigma_{yx} & \sigma_{yy} & \sigma_{yz} \\ \sigma_{zx} & \sigma_{zy} & \sigma_{zz} \end{bmatrix} \tag{15}$$

and **g** is the gravity force. The displacement field *u* can be determined from strains using the stress-strain relationship for the material. These fully coupled equations are solved simultaneously at each mesh point for each time increment until a converged solution is achieved [9].

4.1 Two-Dimensions

4.1.1 Geomtery and Mesh

The model analyzed in two dimensions was an axial cross section of a pellet of nuclear fuel and sheath with a helium filled gap. A mesh of 1360 quadrilateral elements was created and trials were completed for first (1481 nodes) and second (4321 nodes) order elements. Second order elements add midside nodes to all edges of an element. Through the thickness of the sheath four elements were used to accurately determine the stresses and strains within the material [10]. Figure 1 (a) shows the geometry with dimensions and (b) shows the mesh.

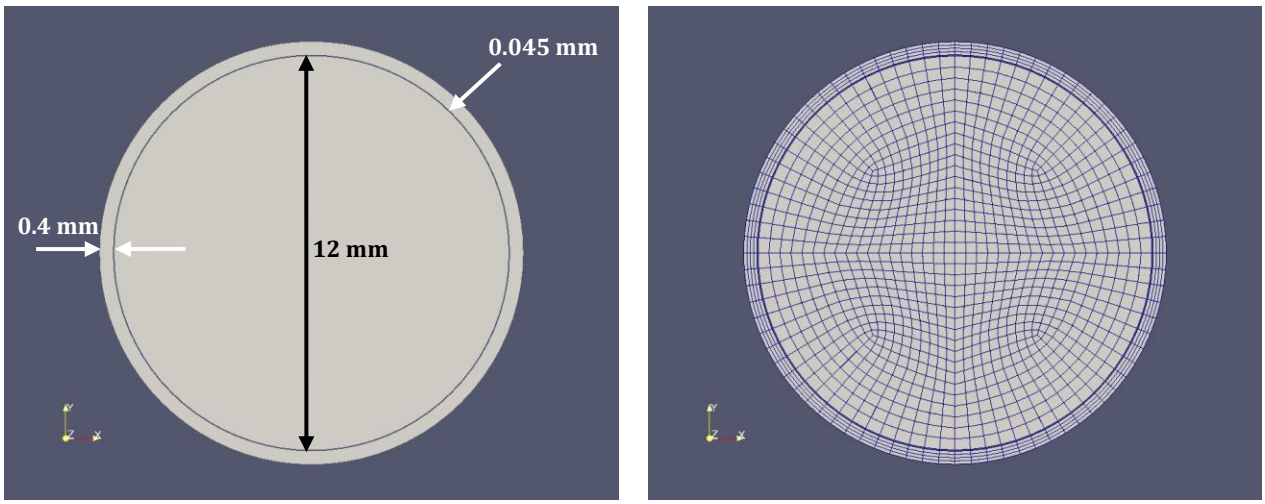

(a) **(b)**

Figure 1: (a) 2D geometry with dimensions, (b) Quadrilateral mesh for 2D contact analysis.

4.1.2 Material Properties

The contact analysis contained three materials, UO_2 fuel, Zircaloy 4 sheath, and helium filled gap. Table 1 provides the material properties used for the fuel and sheath. Note that constant properties are currently used to isolate contact modeling from other effects.

Table 1: Material properties used in 2D contact analysis for UO_2 fuel and zircaloy-4 sheath

Property	Fuel	Sheath
Density (kg m^{-3})	10431.0	6551.0
Young's Modulus (GPa)	180	70
Poisson's Ratio	0.3	0.3
Thermal Expansion Coeffcient (K^{-1})	13.9×10^{-6}	5.7×10^{-6}
Thermal Conductivity (W m^{-1} K^{-1})	3	16
Specific Heat (J $m^{-3}K^{-1}$)	320	330
Linear Power* (kW m^{-1})	45	-

*The linear power was converted to a volumetric heat generation rate applied uniformly within the fuel.

To facilitate convergence and obtain accurate results, suitable boundary conditions are required to accurately model the scenario of interest, as well as to prevent rigid body motion from occuring. Rigid body motion is when the location in space of a body cannot be determined in the finite element solver. To mitigate this, the problem must be sufficiently constrained.

The initial temperature of all bodies was set to 300 K. A convective boundary condition was applied to the outside of the sheath to simulate the coolant. The bulk coolant temperature and the heat transfer coefficient were assumed to be 583 K and 50 000 $Wm^{-1}K^{-1}$, respectively. In addition, a uniform pressure of 10 MPa was applied to the outside of the sheath in the inward radial direction. To sufficiently constrain a problem like this the centre point can be fixed to not move in the the vertical or horizontal directions.

4.2 Three-Dimensions

4.2.1 Geometry and Mesh

Symmetry was used to reduce the computational time required for analysis and therefore a quarter of a fuel pellet and sheath was modeled. Note that the fuel chamfer and dish were ignored at this stage. Three different mesh densities of single order hexahedral elements were used to determine if the same results could be obtained with less nodes. Fewer nodes mean fewer calculations and less computational time. The original mesh contained 6304 nodes and 5100 elements, the half mesh contained 3752 nodes and 2912 elements, and the quarter mesh contained 1992 nodes and 1452 elements. Figure 2 (a) shows the geometry with dimensions for the 3D case and (b) provides an isometric view of the original three-dimensional mesh. The pellet radius, sheath inner and outer radii and intial gap size are the same as the 2D model.

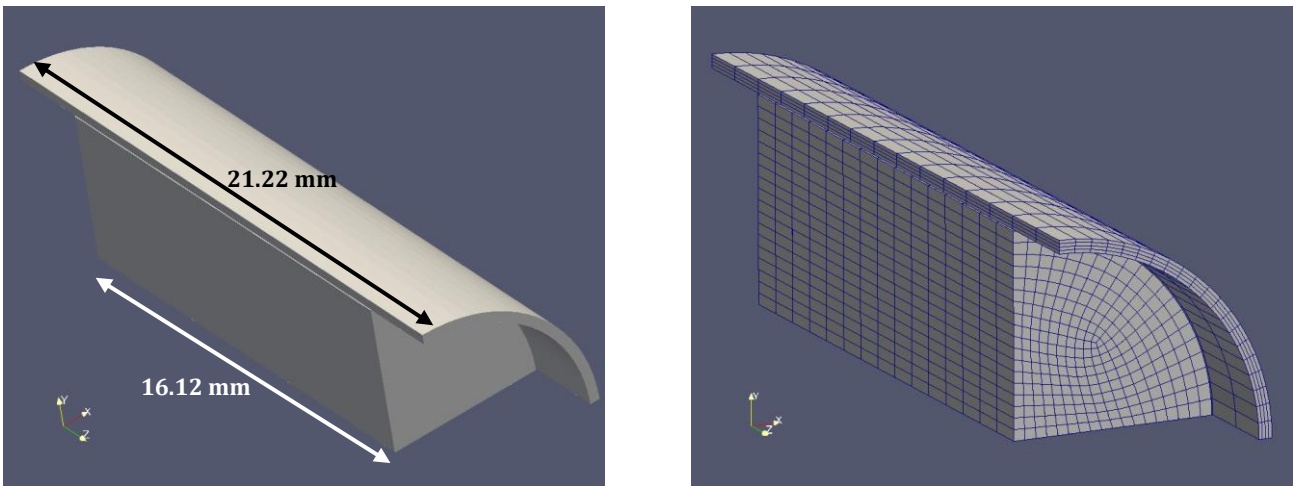

(a) **(b)**

Figure 2: (a) 3D geometry with dimensions, (b) Original mesh for the 3D contact analysis (6304 nodes, 5100 elements).

4.2.2 Material Properties

The material properties used in the three-dimensional case are the same as two dimensions and can be found in Tables 1 and 2.

4.2.3 Boundary Conditions

Since planes of symmtery were employed in the 3D case, additional boundary conditions are required. The same conditions as in 2D were applied to the outside of the sheath. At the vertical symmetry plane, all nodes were constrained to move in the vertical direction as well as the temperature gradient was set to zero across the boundary. Similarly, for the horizontal symmetry planes, all nodes were constrained to move in the horizontal direction. On the front and back faces of the fuel pellet the temperature flux was also set to zero to simulate additional pellets being in contact with these surfaces. Lastly, the corner node at the intersection of the symmetry planes was fixed from moving in the axial direction for the fuel pellet. In addition, the front face of the sheath was fixed from moving in the axial direction to prevent rigid body motion in that direction.

5. Results

Several contact trials were completed to determine the behaviour of the contact algorithm employed in MOOSE and it's affect on temperature and pellet hourglassing. Contact is a transient phenemonon and thus the simulations were run as transient simulations until a steady state solution was achieved. The temperature, pellet hourglassing, and contact behaviour results are presented.

5.1 Temperature

The temperature profile for both the two and three-dimensional cases are as expected. The highest temperature is located at the centre of the fuel pellet and the coolest at the outside of the sheath. The centreline temperature is lower than expected because the gap model is simplified and the material properties are constant. Figure 3 presents the temperature profiles for (a) 2D first order mesh and (b) 3D original mesh.

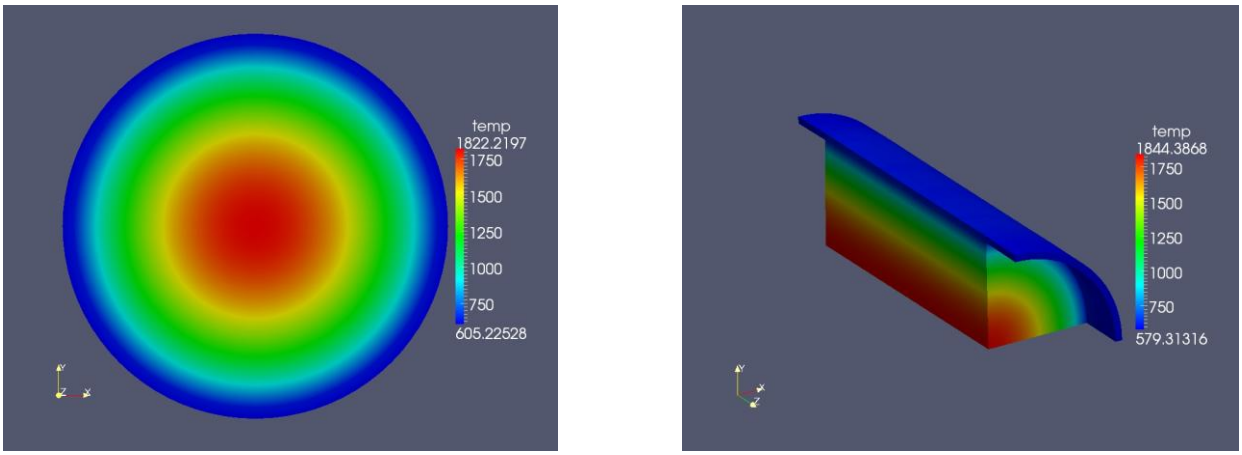

(a) **(b)**

Figure 3: Temperature profiles in Kelvin for (a) 2D, (b) 3D original mesh.

5.2 Pellet Hourglassing

A plot of the y-displacement demonstrates the expected pellet hourglassing in three-dimensions. The behaviour in two dimensions will be similar to the midplane of the fuel pellet in three

dimensions. The hourglassing profile is magnified to show the ridging phenomenon experienced by the pellet. Figure 4 shows the hourglassed pellet. It is encouraging that even with simplified material properties and gap behaviour, the pellet still behaves in the expected manner.

5.3 Contact Algorithm

The contact algorithm employed by MOOSE analyzed in this work is the penalty method. A penalty factor is defined which is used to minimize interpenetration between the two bodies. In penalty contact, the contact force is calculated by adding a fictitious spring between the fuel and sheath where the stiffness of the spring is given by the penalty factor, and the distance the spring is displaced is the interpeneteration of the two bodies. A tangential tolerance is also provided to help extend contact surfaces by a small amount at locations of symmetry to ensure each master node has a corresponding slave surface directly in front of it. The behaviour of the contact pressure and penetration as a function of the penalty factor for all mesh types described is provided.

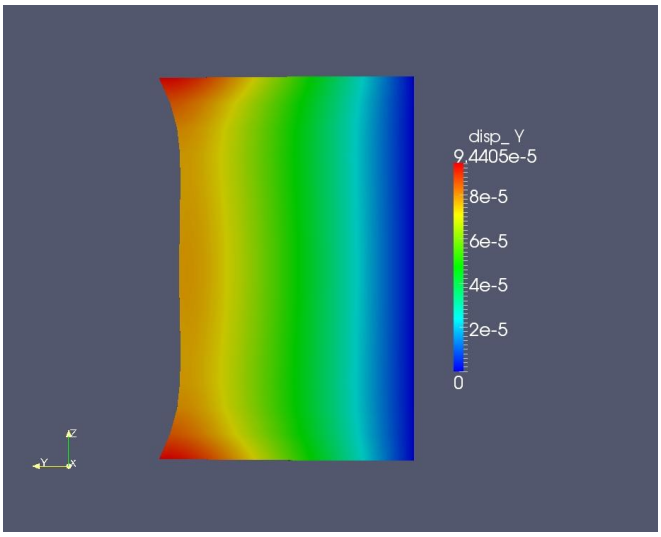

Figure 4: Plot of the fuel pellet exhibiting pellet hour glassing. Deformation in meters is exaggerated.

Table 2 outlines the contact parameters used across the gap. Two forms of contact are required, mechanical contact to ensure stresses and strains are calculated correctly, and thermal contact to ensure that the temperature profile is continuous across the gap.

Table 2: Mechanical and thermal contact parameters

Parameter	Mechanical Contact	Thermal Contact
Penalty Factor	Varies	-
Tangential Tolerance	10^{-4}	-
Gap Conductivity ($Wm^{-1}K^{-1}$)	-	0.15

5.3.1 Contact Pressure

Intuitively, as the penalty factor increases the contact pressure should increase until it reaches a plateau. The value at this plateau should be the contact pressure exerted by one body onto the other. The contact pressure asymptotically approaches a value because pressure between two bodies is constant in reality. In the 2D case this value is approximately 43 MPa. In 3D the midplane value is approximately 25 MPa and the ridge value is approximately 230 MPa. Figure 5 (a)-(d) presents the contact pressure results for the 2D case and the three different mesh densities in 3D. In the 2D case it can be seen that the second order trials approached the asymptotic limit slightly faster then the first order mesh. However, due to convergence issues, results at higher penalty functions could not be obtained and the 2nd order mesh never does reach the value of approximately 43 MPa. The 3D cases have two contact pressures, one for the ridge (ends) of the pellet and one for the midplane. The midplane pressure is about half of what was calculated in 2D. The contact pressure at the ridges is expected to be slightly higher than at the midplane. The pressure at the ridges are approximately 10 times higher than at the midplane, much higher than expected. Investigation is currently underway to improve the contact pressure results of the model at the ridge locations. The midplane pressure is about half of what was calculated in 2D, which is reasonable. The converged contact pressure for all 3D simulations seem to be independent of mesh density. However, the more coarse the mesh the higher penalty factor that can be used. In addition, computational requirements are greatly reduced using a quarter mesh compared to the original mesh.

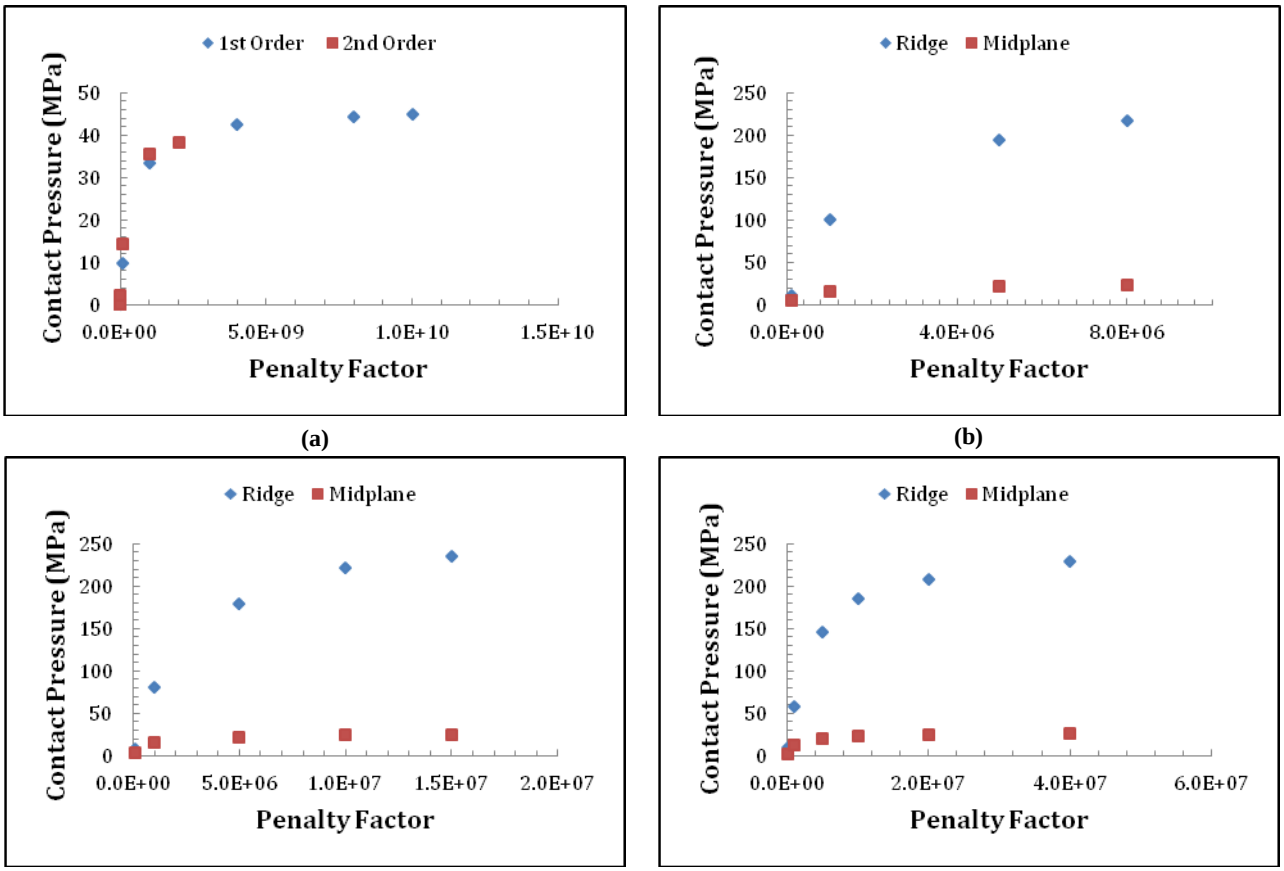

Figure 5: Contact pressure as a function of penalty factor for (a) 2D, (b) 3D original mesh, (c) 3D half mesh, (d) 3D quarter mesh

5.3.2 Penetration

Interpenetration between the fuel and sheath is inversely proportional to the penalty factor. As the penalty factor increases the penetration is supposed to asymptotically approach zero. Figure 6 (a)-(d) presents the penetration response to penalty factor for the 2D case and three mesh densities in 3D. Similarly to contact pressure, the 3D cases have both a penetration at the ridge location and midplane location. The results for the 2D case are as expected and verified by hand calculations. In 3D, the penetration results are reasonable at the midplane location but are higher than expected at the ridges. Investigation is currently underway to improve the model to produce more accurate results at the ridge locations. The desired result is to have the peneteration less than two microns as this is within the surface roughnesses of the fuel and sheath. For the 3D simulations, the ridge penetration is expected to be higher than at the midplane, as observed. Stresses and strains will be higher at the ridge locations and lead to sheath bambooing.

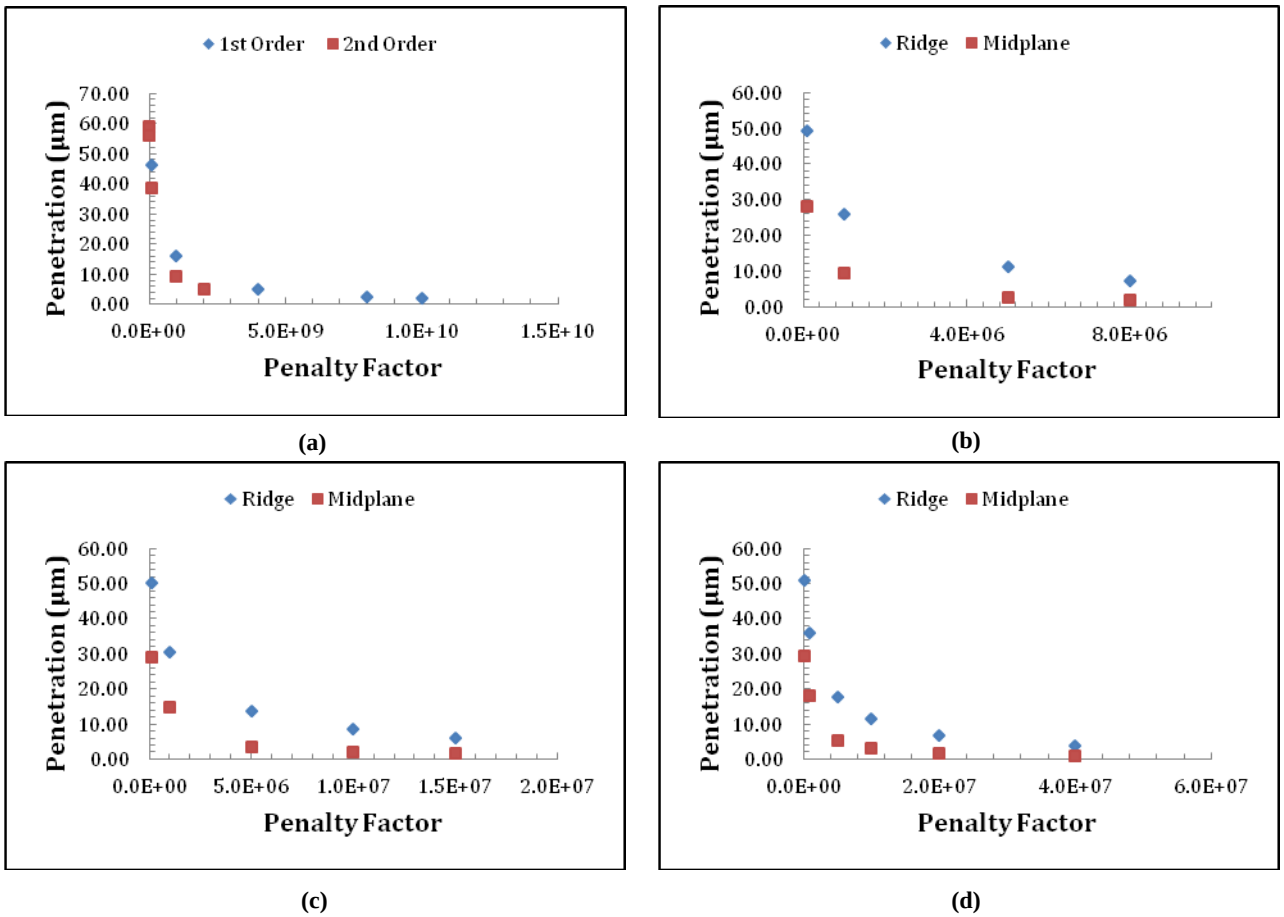

Figure 6: Penetration as a function of penalty factor for (a) 2D, (b) 3D original mesh, (c) 3D half mesh, (d) 3D quarter mesh

6. Future Work

The analysis of the contact algorithm was the first step in the overall feasibility study of modeling CANDU fuel using Idaho National Laboratory's MOOSE framework. Isolation of contact is no longer required. The next steps are outlined below

- Fuel and sheath material properties need to depend on temperature. The pellet-to-sheath heat transfer coeffcient needs to depend on the gap size and gas pressure when the gap is open, or the interface pressure when the gap is closed. The heat generation is another parameter and will be time-dependent. Temperature, displacement and stress results will be obtained.

- Next, additional pellets are added to the full three-dimensional model two at a time until a full fuel element is generated. The expected additional challenge of this second phase is the additional contact pairings introduced between the individual pellets.

- The final phase of this feasibility study is to begin adding additional fuel pheneomena that affects the temperature and stress strain results including, fuel swelling and densification, fuel and sheath thermal and irradiation creep, burnup, and fission gas production and release.

- To benchmark the results obtained from HORSE simulations, comparisons will be made with the current ANSYS deformation model developed by Williams. Additional comparisons will be completed against ELESTRES-IST which has been validated against experiments.

7. Conclusions

In this work, the contact algorithm within INL's MOOSE was investigated. Temperature, pellet hourglassing, contact pressure and penetration results were presented and were as expected except for the penetration and contact pressure at the pellet ridges. Ridge and midplane effects produce differing results between these two locations in the 3D cases. The next steps of the feasibilty study have been outlined and the capabilities of MOOSE are promising for predictive modeling of CANDU fuel.

8. Acknowledgements

The authors would like to thank the MOOSE developers at Idaho National Laboratory for providing the computational framework used in this work, and NSERC for funding.

9. References

[1] A. Prudil, B.J Lewis and P. Chan, "Development of the FAST Code for Modelling CANDU Fuel", Proceedings of the 33rd Annual Conference of the Canadian Nuclear Society, Saskatoon, Saskatchewan, Canada, 2011 June 10-13

[2] J.S. Bell and B.J Lewis, "CANDU fuel bundle deformation modeling with COMSOL Multiphysics", Journal of Nuclear Engineering and Design, Vol. 250, 2012 pp. 134-141.

[3] A. Williams, Personal Conversation, Chalk River, Ontario, Canada, August, 2012

[4] D.A. Knoll and D. E. Keyes, "Jacobian-free Newton-Krylov methods: a survey of approaches and applications," Journal of Computational Physics, Vol. 193, 2004, pp. 357-397

[5] V. Mousseau, "Implicitly balanced solution of the two-phase flow equations coupled to nonlinear heat conduction," Journal of Computational Physics, Vol. 200, 2004, pp. 104-132
[6] V. A. Mousseau, D. A. Knoll and W. J. Rider, "Physics-Based Preconditioning and the Newton-Krylove Method for Non-equilibrium Radiation Diffusion," Journal of Computational Physics, Vol. 160, 2000, pp. 743-765
[7] S. Balay, J. Brown, K. Buschelman, V. Eijkhout, W. Gropp, D. Kaushik, M. Knepley, L. Curfman McInnes, B. Smith and H. Zhang, "4.4 Preconditioners," in PETSc Users manual Revision 3.3, chicago, Mathematics and Computer Science Division, Argonne National Laboratory, 2012, pp. 78-85
[8] D. Gaston, C. Permann, D. Anders, J. Peterson and J. Miller, MOOSE Training Workshop, Chicago, 2013
[9] R. Williamson, S. Novascone, J. Hales, B. Spencer, G. Pastore and D. Perez, "2 Governing Equations," BISON Theory Manual, Idaho Falls, Fuels Modeling & Simulation Department, Idaho National Laboratory, 2012, p.5
[10] Dassault Systemes, "4.1.2 Reduced Intergration," Daussault Systemes, Providence, 2011